Characterization of the Temporal Response Profile of Carbon Black−Polymer Composite Detectors to Volatile Organic Vapors

Shawn M. Briglin and Nathan S. Lewis*

Noyes Laboratory, 127-72, Division of Chemistry and Chemical Engineering, California Institute of Technology, Pasadena, California 91125

Received: February 18, 2003; In Final Form: May 20, 2003

The relative differential resistance responses of carbon black−poly(ethylene-*co*-vinyl acetate) (PEVA) composite vapor detectors were evaluated in response to short rise time (<2 ms for a 17 ms pulse length) square pulses of acetone, *n*-hexane, methanol, 2-propanol, or toluene, in a background of synthetic air. The use of ultrathin films, along with a rapid vapor delivery system, facilitated measurement of the rapid time response available from this exemplary carbon black−polymer composite chemiresistive film for the detection of common organic vapors. Detectors formed from very thin (<200 nm) PEVA−carbon black composites produced steady-state responses within 17 ms upon exposure to methanol and produced steady-state responses within 90 ms upon exposure to toluene, acetone, and *n*-hexane. In accord with Fickian diffusion, the response times of the relative differential resistance of PEVA−carbon black detectors to analyte exposures were proportional to the square of the film thickness, l, in the range $510 \leq l \leq 5700$ nm. Additionally, the relative differential resistance versus time profiles of PEVA−carbon black detectors were well fit by a simple finite difference model based on Fickian analyte diffusion, using a single analyte diffusion coefficient, for a variety of different film thicknesses and analyte concentrations.

I. Introduction

Vapor detectors that exploit sorption of an analyte into a polymer film have received significant attention in the recent literature. Such detectors include carbon black−insulating polymer composites,[1] conducting organic polymers,[2−4] polymer-coated quartz crystal microbalances (QCMs),[5] polymer-coated surface acoustic wave devices (SAWs),[6,7] polymer-coated capacitors,[8] and dye-impregnated polymeric beads or coated optical fibers.[9−11] The different signal outputs produced by all of these detectors result from the differing types of signal transduction mechanisms exploited by each of the various sensor modalities. For example, carbon black composites measure the sorption-induced resistance change as a result of swelling of the polymer film,[12] QCM measures the frequency shift of the crystal as a result of sorption-induced changes in mass and modulus of the polymer film,[13] and dye-impregnated polymeric beads measure solvatochromic changes in response to a combination of sorption-induced local solvation changes and gross structural changes of the polymer matrix.[14] Differences in response time and response magnitude between various sorption-based detector types therefore should primarily involve differences arising from the mode of signal transduction and the sensitivity and temporal response behavior of the signal readout apparatus, as opposed to differences in the fundamental process of time-dependent sorption of a particular analyte vapor into a given type of polymer film.

Recent work in our laboratories has focused on chemically sensitive vapor detectors formed by the dispersion of electrically conductive carbon black particles into a range of insulating organic polymers.[1] The swelling of these films during the sorption process produces a dc electrical resistance change, and simple spray-coating deposition methods permit the fabrication of such chemiresistor-type vapor detectors in a wide range of geometries and film thicknesses. To date, studies have focused primarily on the steady-state relative differential resistance response:

$$\Delta R^{eq}/R^{i} = (R^{eq} - R^{i})/R^{i} \quad (1)$$

where R^{i} is the initial resistance of the detector in the absence of analyte and R^{eq} is the resistance after the detector has reached equilibrium in the presence of a constant concentration of analyte vapor. This $\Delta R^{eq}/R^{i}$ value is often used as the response descriptor because it is relatively insensitive to the method of introducing the vapor to the detector.[1] An additional advantage of analyzing the steady-state $\Delta R^{eq}/R^{i}$ response is that, for typical carbon black−polymer composite vapor detectors, this descriptor has been shown to be a linear function of analyte concentration,[15] which is a requirement for many signal processing approaches and for the additivity of signals in response to multiple analytes.[15,16] Use of the steady-state $\Delta R^{eq}/R^{i}$ signal also minimizes the sensitivity of the detector response to many process-related variables such as the concentration of carbon black in the composite or to variations in film thickness either between detectors or in an individual detector.[15] Finally, use of the steady-state response allows optimization of the geometry and form factor of the vapor detectors to facilitate operation at optimal signal-to-noise ratios for detection of a specific analyte of interest.[17]

In this work, we have explored the temporal response of the signals produced by carbon black−polymer composite vapor detectors during exposure to well-defined, short rise time pulses of analyte vapors. Traditionally, achieving rapid steady-state detector responses and investigating quantitatively the short time vapor detector response properties have required construction

* To whom correspondence should be addressed.

10.1021/jp030218i CCC: $25.00
Published on Web 09/16/2003

of an apparatus that has rapid vapor mixing capabilities, low dead volumes in the delivery system, and synchronization between the timing of the vapor delivery to the detector and the timing of the detector output measurement and data acquisition system.[18,19] Using such an approach, we have previously demonstrated detection of 0.2 ppb of 2,4-dinitrotoluene in an ambient air background in <5 s using a poly(methyloctadecylsiloxane)−carbon black detector.[20] We describe herein the construction of an apparatus that instead utilizes rapid switching between a steady-state vapor stream and an analyte-free background stream, permitting the generation of much shorter rise time, square pulses of analyte vapor. The system is calibrated using optical detection of the time-dependent analyte concentration in the region adjacent to the vapor detector. Using this experimental approach, the response times of films of varying thickness were determined with respect to the time response of the experimental system. The films studied were carbon black−PEVA composites, and the thinnest detector in our test set exhibited responses to steady-state in <17 ms for methanol, and response times to steady-state in <90 ms for all of the analyte combinations investigated. We additionally demonstrate that, at least for the PEVA−carbon black detectors explored in this work, a simple model based on Fickian diffusion is adequate to explain the full time response of the detector, including both the sorption and desorption processes. Hence, if desired, even more rapid analyte detection can be achieved though analysis of the detector data produced prior to attainment of the steady-state response condition. Finally, we show that this time response can provide additional information on the identity of an analyte beyond that available in the equilibrium response alone.[9−11,14,19]

II. Theoretical Considerations

The time course of sorption and desorption of small permeant molecules into certain polymers can be described using Fick's second law of diffusion:[21,22]

$$\frac{\partial C}{\partial t} = D\frac{\partial^2 C}{\partial x^2} \tag{2}$$

where C is the analyte concentration in the polymer, t is time, D is the polymer/analyte diffusion coefficient, and x is the space coordinate. When the behavior of small analyte molecules permeating through low glass transition temperature, T_g, polymers is well-described by a single, concentration-independent value of D, these systems are designated as Fickian.[22] Crystalline polymers having high T_g values often exhibit complicated sorption and desorption phenomena, possibly resulting from plasticization of the polymer induced by the presence of the permeant. A description of the permeant sorption behavior in such systems typically requires concentration-dependent diffusion coefficients or may require even more complicated approaches.[21,23,24]

To model the time response of a sorption-based polymer film detector, the film can be represented as an isotropic planar sheet of thickness l, allowing use of the one-dimensional diffusion equation, eq 2, to describe the concentration of analyte in the film, $C(x,t)$, where the space coordinate, x, is the direction normal to the surface of the polymer film. During exposure to a pulse of analyte vapor of concentration $C_{vap}(t)$, the surface of the detector film is assumed to reach equilibrium instantaneously with the analyte vapor concentration. Thus, the time-variant boundary condition at this interface is

$$C(l,t) = KC_{vap}(t) \tag{3}$$

where K is the vapor/film equilibrium partition coefficient. The detector/substrate interface ($x = 0$) is assumed to be impervious to analyte and thus serves as a point of zero analyte flux:

$$dC(0,t)/dx = 0 \tag{4}$$

Although analytical solutions are attainable for eq 2 in special cases, such as for perfectly square vapor pulses,[21] a more versatile approach is to express eq 2 in terms of finite differences and to evaluate the resulting initial value problem numerically. A well-established method is to use the Crank−Nicholson implicit scheme:[21,25,26]

$$\frac{c_{n,j+1} - c_{n,j}}{\Delta T} = \frac{D}{2}\left[\frac{(c_{n+1,j+1} - 2c_{n,j+1} + c_{n-1,j+1})(c_{n+1,j} - 2c_{n,j} + c_{n-1,j})}{(\Delta X)^2}\right] \tag{5}$$

where ΔX is the distance interval and ΔT is the time step in the simulation.

Following this method, the thickness of the detector film is divided into N internal grid points ($n = 1, 2, 3, ..., N-1, N$) with the nth grid point located at the position $x = (l/N)(n-1) = \Delta X/(n-1)$. After establishing the initial values of each grid point at the first time step, $j = 0$, then for each successive time step, $j + 1$, the N unknown analyte concentrations are found from the set of N simultaneous equations.[25,26] The boundary conditions of eqs 3 and 4 are readily included for each time step at the external grid points $n = N + 1$ ($x = l$) and $n = 0$ ($x = 0$).

In most studies of polymer sorption, the concentration of permeant is integrated across the polymer thickness to produce an expression for the total mass of the permeant in the polymer film as a function of time. This approach is used because the relative mass uptake of the polymer film during sorption and desorption is the most often measured experimental quantity. However, to describe the time dependence of the resistance of a carbon black−polymer composite film vapor detector, $R(t)$, the relative location of analyte in the film must be evaluated. In an extension to the finite difference treatment of analyte sorption into a polymer film outlined above, the film is therefore represented at each time step as a network of N parallel resistances ($n = 1, 2, 3, ..., N-1, N$), thereby allowing computation of the total film resistance, R_j, at time step j. This division of the film at each time step into a network of electrically parallel resistances follows from the assumption that the resistance of the thin polymeric detector film is to be measured along an axis normal to the film's thickness (and thus normal to the space coordinate x).

The resistance at each of these grid points can be expressed as two resistive components in series. The first component is independent of analyte concentration and, assuming uniform resistivity throughout the film, is identical for each of the N internal grid points. This resistance, r^i, is the value of the resistance in each of the N lamellae of the simulation, which for resistors in parallel is simply given by

$$r^i = NR^i \tag{6}$$

The second series component at each grid point is the concentration-dependent resistance in an individual lamella of the simulation, $r_{n,j}$. This resistance equals 0 in the absence of

analyte and is the value of the film resistance that changes upon exposure of the film to analyte vapor. At equilibrium, this quantity can be expressed as

$$r_{n,j} = N\Delta R^{eq} \quad (\text{for } j \text{ at equilibrium}) \tag{7}$$

where $\Delta R^{eq} = R^{eq} - R^{i}$. Because the resistance response of a carbon black−polymer composite detector is linearly related to the concentration of analyte in the polymer film,[12,15] the concentration-dependent portion of the parallel resistance at grid point n at time step j is thus

$$r_{n,j} = N(C_{n,j}/C^*)\Delta R^{eq} \tag{8}$$

where C^* is the concentration of analyte in the film at equilibrium and $C_{n,j}$ is the concentration of analyte in the nth lamella at time step j. The value of C^* is related to the maximum concentration of analyte in the vapor pulse, C_{vap}^*, as $C^* = KC_{vap}^*$. Because a network of parallel resistances adds reciprocally, the macroscopically measured sum of these two components of resistance in each lamella, combined across the full detector thickness at time step j, is given by

$$R_j = \frac{1}{\sum_{n=1}^{N} \frac{1}{r^{i} + r_{n,j}}} \tag{9}$$

After substitution with eqs 7 and 8, eq 9 can be written as

$$R_j = \frac{1}{\frac{1}{N}\sum_{n=1}^{N} \frac{1}{R^{i} + \Delta R^{eq} C_{n,j}/C^*}} \tag{10}$$

Evaluation of eq 10 for each time step of eq 5 provides a simple finite difference model for the resistance versus time response of a carbon black−polymer composite vapor detector in response to an arbitrarily shaped pulse of analyte.

III. Experimental Section

A. Materials. Poly(ethylene-*co*-vinyl acetate) with 33% acetate (PEVA) was purchased from Scientific Polymer Products. The solvent *n*-hexane was purchased from Aldrich Chemical Corp., while the solvents acetone, toluene, 2-propanol, and methanol were purchased from EM Science. All solvents were used as received.

B. Fabrication of Substrates and Detector Films. *1. Substrates.* Glass microscope slides were cut into 5.0 cm long, ≈0.29 cm wide rectangular strips. A "T" shaped region that extended over the full face of each glass strip was masked off, and the glass strips were coated with a 30 nm layer of adhesion-promoting evaporated Cr followed by 50−70 nm of evaporated Au. This process produced two parallel 3.0 cm long metal contact regions that were separated by a 0.1 cm uncoated gap. These substrates were used for all measurements performed in this work except for experiments on detectors that were fabricated from the very thinnest films. To maintain moderately low resistance values for the ultrathin detector films, 7 interdigitated Au/Cr fingers were patterned onto one of the glass strips using a standard subtractive lithographic process. This electrode pattern produced 12 parallel contacts separated by gaps of 200 μm.

2. Fabrication of Detector Films. Suspensions of carbon black−polymer composites were prepared by dissolving 160 mg of polymer in 20 mL of toluene, followed by addition of 40 mg of carbon black (Black Pearls 2000, Cabot).[1] The mixtures were sonicated for 10 min and were then sprayed directly onto the Au/Cr glass substrates using multiple lateral passes of an airbrush (Iowata HP-BC) held at 6−14 cm above the substrate. The number of passes varied from 5 to >50, depending on the desired film thickness. The area of the carbon black−polymer films in the region between the two parallel electrodes varied slightly from film to film, with the length of this 0.1 cm wide rectangular film region ranging from 0.6 to 1.2 cm. These rectangular regions of film did not span the entire length of the electrodes. The thickness of each detector film was measured as the average of several traces of a mechanical stylus profilometer (model 3030, Sloan Dektak). Five different film thicknesses were studied in depth: 510 nm thick films having resistances of ≈14 kΩ, 870 nm thick films with resistances of 12 kΩ, 1030 nm thick films with resistances of 8.8 kΩ, 5700 nm thick films with resistances of 1.7 kΩ, and an ultrathin (<200 nm thick) film having a resistance of 670 kΩ.

C. Analyte Vapor Generator. An automated flow system was used to generate a diluted stream of solvent vapor.[27] The carrier gas was oil-free air obtained from the house compressed air source (1.10 ± 0.15 parts per thousand (ppth) of water vapor) controlled with a 28 L min^{-1} mass flow controller (model 1660, Unit). To obtain the desired concentration of analyte in the gas phase, a stream of carrier gas controlled by a 625 mL min^{-1} mass flow controller was passed though one of five bubblers. Saturation of the gas flow through the bubbler of interest was confirmed with a flame ionization detector (model 300 HFID, California Analytical Instruments, Inc.). Mixing of the two streams produced analyte vapor at the desired value of $P/P°$, where P is the partial pressure of the analyte and $P°$ is the vapor pressure of the analyte at ambient temperature. The temperature during data collection was 293 K, and the temperature of the bubblers was controlled by immersing the solvent bubblers in a tank of water regulated with a constant temperature water circulator (Haake DC5/K20).

D. Detector Chamber. *1. Interface to Vapor Delivery System for Rapidly Switching between Background Air and Diluted Analyte Vapor Streams.* Scheme 1a depicts the low-volume vapor sample chamber that contained a mechanism for rapidly switching between two vapor streams. The purpose of the device was to quickly switch the headspace over the detector film between either a stream of background carrier gas or a stream of identical carrier gas which also contained an analyte vapor at a predetermined concentration. The airflow in this sample chamber was directed using two concentric channels. The 7.3 cm long inside channel (Scheme 1b) was partially formed from a quartz cuvette (model 3-3.45-Q-3, Starna, Atascadero, CA) that was cut open at both ends. This inside channel had 0.125 cm thick walls and had an internal cross section of 0.3 cm × 0.3 cm. A 5.0 cm long × 0.29 cm wide Au/Cr glass substrate coated with a carbon black−polymer composite film was inserted along the floor of the inside channel until the substrate was flush with one end of the quartz channel and extended 0.7 cm farther into an Al extension of the inside channel. Electrical contacts to the leads on the substrate were made in this channel. The presence of this 0.10 cm thick substrate reduced the cross section of the headspace of the chamber to approximately 0.2 cm × 0.3 cm. This inside channel extended for a total length of 7.3 cm including both the quartz and Al regions. A connection

SCHEME 1: (a) Perspective View of the Low Dead Space Chamber Developed for These Experiments, (b) Vertical Cross Section through the Chamber at Two Different Rotational Positions of the Shutter Device,[a] and (c) Schematic of the Aluminum Chopper Disk Which Was Used for Switching the Analyte Concentration in Proximity to the Detector[b]

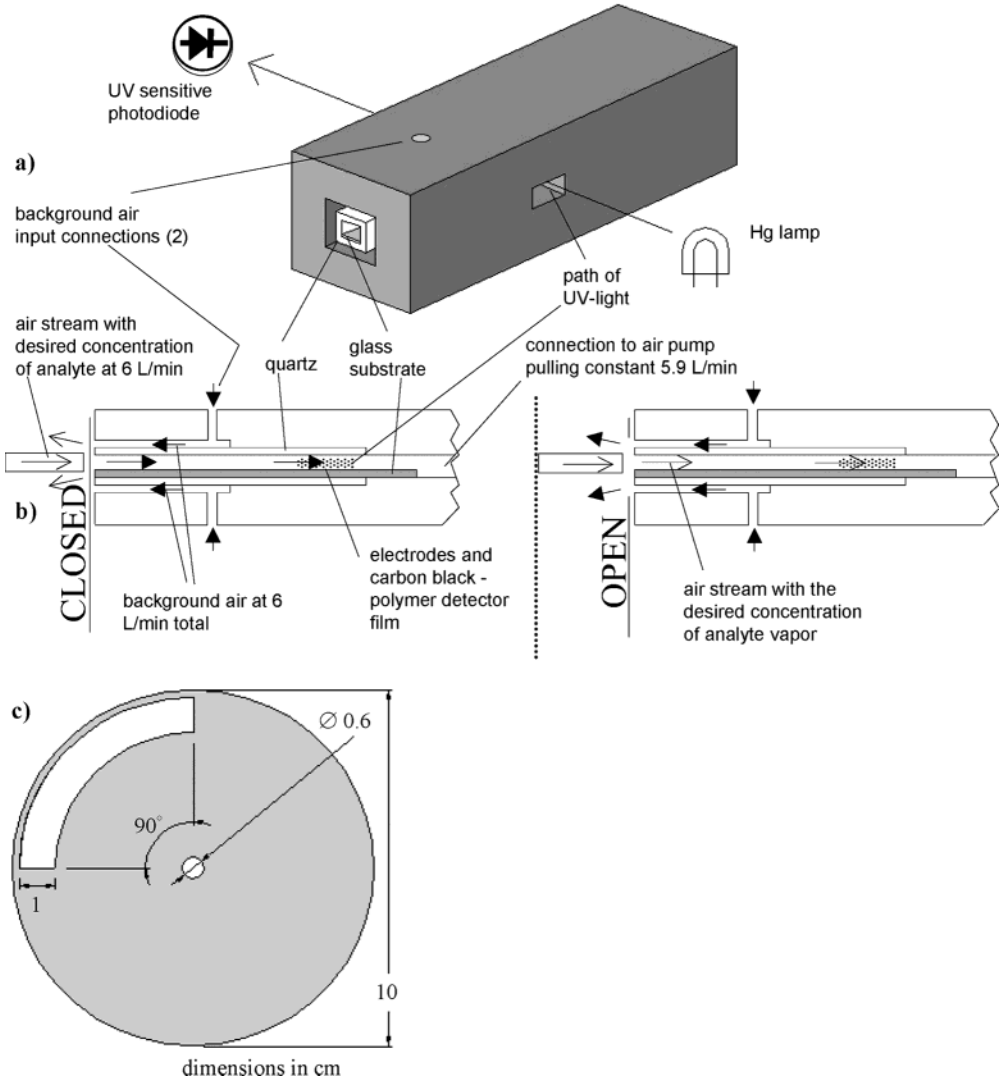

[a] This shows the operating principle used to quickly switch the detector ambient between two air streams. [b]The 25% open fraction of the disk results in an exposure duty cycle of 25%.

to an air pump was made at the end of the Al section of this channel. The purpose of this pump, which was equipped with a flow regulator (model 034-62G, Aalborg Instruments), was to pull air at a constant volumetric flow rate of 5.9 L min^{-1} through the inside, detector containing, channel at all times. A second channel, the outside channel, surrounded part of the quartz section of the inside channel and also remained open at the same end as the inside channel. This outside channel was machined from Al and had walls with an internal cross section of 0.82 cm × 0.82 cm that were each 0.185 cm from the outside walls of the quartz channel.

The output port from the analyte vapor generator described above was positioned adjacent to the exposed opening of the inside quartz channel and was separated from this opening by a distance of ≈0.2 cm. A circular aluminum disk (Scheme 1c) of dimensions 0.1 cm thick and 10.0 cm in diameter was placed between the output port of the vapor delivery system and the opening of the inside channel. This disk was similar in concept to an optical chopper wheel having a single opening. In actuality, to keep the wheel balanced, the chopper disk was machined to have two such holes symmetrically positioned on the wheel, and one hole was covered with a thin piece of aluminum foil to prevent air flow through that section of the wheel. The chopper wheel was connected to an LED/photodiode trigger and was rotated through use of either of two differing range, variable speed dc gear motors (Pittman, Harleysville, PA).

The spinning disk was positioned to permit the flow from the vapor source into the channel only when the vapor encountered the opening in the wheel (25% open, 75% closed). The pump connected to the inside channel drew a constant 5.9 L min^{-1} of air regardless of the open/closed state of the chopper wheel. A third mass flow controller was used to supply background air at a constant flow of 6 L min^{-1} to the outside channel (Scheme 1b). When the disk blocked the inside channel from the vapor source, the pump pulled air from the outside channel. This air flowed through the outside channel in a direction opposite to that of the air being pumped through the inside channel, and when this background stream was not being drawn into the inside channel, it simply flowed away from both openings. A 0.1 L min^{-1} excess of vapor generator output over the pump rate input into the inside channel ensured that a sufficient quantity of analyte vapor was available for the pulse without significant mixing of the pulse vapor with additional background air. A different spinning rate was chosen for the

SCHEME 2: (a) Schematic of the Instrumentation and Electrical Connections Used in the Experiments with the Chopper Used To Generate Short Pulses and (b) the Solenoid Used in Slower Experiments with Thicker Films To Switch Analyte across the Detector

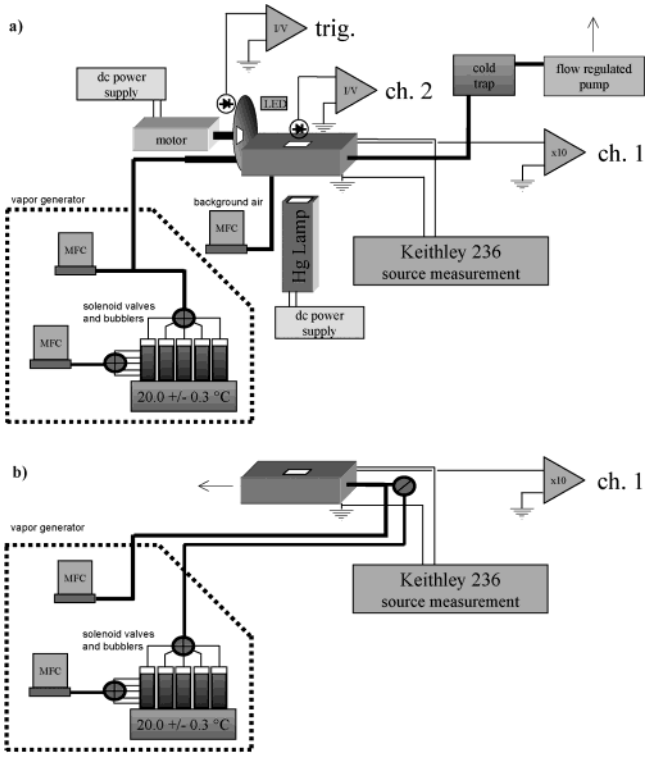

chopper wheel for each polymer/analyte combination. The value was chosen to provide a pulse of analyte just long enough that the detector response leveled off at a steady-state by the end of the pulse. Shorter pulses did not ensure that the film reached equilibrium with the headspace, whereas longer pulses did not produce optimally fast rise times of the leading edge of the vapor pulse onto the detector film.

2. Lower Speed Pulses of Analyte. For thick films that displayed response times of >3 s, the gas chopper was not required and a Teflon diverting solenoid valve was instead sufficient to switch analyte vapor into the gas flow. The gas stream was connected directly to the low dead space chamber, and to initiate the pulse, a diverting solenoid upstream from the entrance of the chamber was switched open, thereby adding saturated analyte vapor to the background stream. In this setup, the total flow rate over the detector was held constant at 6.0 L min^{-1} before, during, and after exposure to the analyte of interest.

E. Direct Current Resistance Measurements. Resistance measurements of the detectors were obtained with a source measurement unit (Keithley model 236) that supplied a constant current through the detector film (Scheme 2a). The voltage drop across the detector was dc-coupled into a high input impedance (100 MΩ) FET input preamplifier (SR560, Stanford Research Systems) which amplified the signal with a gain of 10:1. This voltage was then dc-coupled into either an oscilloscope (TDS 210, Tektronix) or a digital multimeter (Keithley model 2002) depending on the time response of the signal. The sample chamber that housed the detector and all cabling was fully shielded. The bandwidth of the Keithley current source was only 100 Hz ($f_{bw} = -3$dB) which, although adequate for the more slowly responding (thicker) detectors, would attenuate some of the higher frequency components in the responses of the thinnest and most rapidly responding detectors. A higher bandwidth current source was therefore required for measurements of the temporal response of the ultrathin detector films. This constant current source was an 18 V battery connected in series to a resistance of 40 MΩ. This arrangement did not attenuate the important higher frequency components that produced the shape of the signals recorded from the most rapidly responding detectors.

Because the vapor pulses were repeated with each rotation of the chopper wheel, between 8 and 64 exposures were averaged on the oscilloscope to produce each recorded data trace for a given experiment. The thickest carbon black−polymer composite films produced responses that were too slow to use the chopper and oscilloscope setup, so the multimeter was used to collect a data stream of the detector response versus time for each analyte exposure to such films (Scheme 2b). When the multimeter was used, no averaging was required because the multimeter has a significantly reduced bandwidth, and as expected, the thicker, larger volume films exhibited lower noise than did the thinner detector samples of the same film area.

F. Optical Monitoring of the Probe Pulse. A low-pressure Hg lamp (model UVG-4, UVP Inc., Upland, CA) was used for illumination. The light source made use of a short-pass filter to attenuate most light with wavelengths longer than the 253.7 nm Hg line. For stability the lamp was modified to run off of several lantern batteries wired in parallel. The light source was placed ≈15 cm from the substrate housing, and light was directed through the 1.0 cm × 0.3 cm entrance slit in the side of the Al sample chamber (Scheme 1a). The light passed through the quartz walls of the inside chamber with a path length of 0.3 cm and passed out an identical 1.0 cm × 0.3 cm exit slit in the opposite side of the Al sample chamber. A UV-sensitive silicon photodiode (UV50, UDT Inc.) was connected to this exit port to capture the light passing through the device. The unbiased photodiode was connected to a JFET input opamp (LF 355, National Semiconductor) configured as a current-sensitive amplifier with a trans-impedance ratio of 5×10^6 V/A and a bandwidth of 6 kHz. The voltage output of this amplifier stage was dc-coupled to the second (channel 2) input on the oscilloscope.

Before initiating a given experiment, a shutter between the lamp and input slit was adjusted to regulate the amount of light passing through the quartz tube and reaching the photodiode. This was necessary to ensure that the output of the current-sensitive preamplifier did not exceed the 2 V offset capability of the oscilloscope. The photodiode current was converted into an absorbance, *A*, which is proportional to the concentration of the analyte in the small headspace above the detector film at a given time. The value of *A* was not converted into a concentration of analyte because neither the exact distribution of the spectral lines nor the exact path length of the uncollimated light source were known. Absorbance data appearing in the figures were first smoothed slightly with a running average filter of 10 data points.

Simultaneous measurement of both the absorbance of the analyte vapor above the carbon black−polymer detector and the resistance response of the carbon black−polymer detector film was only possible for the two analytes, acetone and toluene, that possess moderate absorption cross sections at the 253.7 nm wavelength of the light source. To provide an optical confirmation of the concentration profile of the vapor pulse, experiments using other analytes were preceded immediately before, or repeated immediately after, with identical flow rates and experimental configurations but with the nonabsorbing analyte

TABLE 1: Parameters for, and Results of, Comparisons between Time Profiles of Calculated Responses and the Experimental Responses of Four Different Film Thickness PEVA Detectors

				$P/P^0 = 0.070$								$P/P^0 = 0.040$							
				fit[a]		full fit[b]						fit[a]		full fit[b]					
thickness (nm)	analyte	pulse length (s)	grid pts, N	M	GOF	M	GOF	D^e	$\Delta R^{eq}/R^i$	A^c	t_r^d (s)	M	GOF	M	GOF	D^e	$\Delta R^{eq}/R^i$	A^c	t_r^d (s)
510	methanol	0.14	40	723	0.013	2500	0.012	5.1	0.0072		0.10	723	0.017	2500	0.018	5.1	0.0041		0.10
	acetone	0.38	40	950	0.011	2500	0.013	1.7	0.0279	0.0046	0.31	950	0.013	2500	0.017	1.6	0.0148	0.0027	0.32
	2-propanol	0.92	40	914	0.014	2500	0.014	0.8	0.0135		0.62	914	0.016	2500	0.015	0.8	0.0074		0.68
	hexane	0.92	40	914	0.011	2500	0.012	1.0	0.0481		0.50	914	0.020	2500	0.017	1.0	0.243		0.51
	toluene	0.92	40	914	0.011	2500	0.017	0.78	0.120	0.01052	0.67	914	0.010	2500	0.012	0.83	0.0540	0.0058	0.63
870	methanol	0.38	40	944	0.031	2500	0.036	5.8	0.0057		0.26	944	0.043	2500	0.047	5.6	0.0030		0.27
	acetone	0.99	40	987	0.014	2500	0.016	2.0	0.0288	0.0050	0.76	987	0.019	2500	0.019	2.0	0.0153	0.0028	0.77
	2-propanol	1.75	40	875	0.018	2500	0.017	1.0	0.0125		1.5	875	0.034	2500	0.032	1.0	0.0068		1.5
	hexane	1.22	40	1223	0.029	2500	0.022	1.1	0.0475		1.4	1223	0.031	2500	0.026	1.1	0.0246		1.4
	toluene	1.47	40	738	0.024	2500	0.015	0.94	0.1197	0.01021	1.6	738	0.025	2500	0.015	0.94	0.0553	0.00558	1.6
1030	methanol	0.47	40	1174	0.032	2500	0.031	8.1	0.0059		0.26	1174	0.040	2500	0.041	8.0	0.0030		0.26
	acetone	1.18	40	1176	0.023	2500	0.019	2.5	0.0271	0.0046	0.83	1132	0.034	2500	0.025	2.3	0.0139	0.0018	0.91
	2-propanol	2.20	40	1101	0.023	2500	0.026	0.95	0.0122		2.2	1113	0.027	2500	0.032	0.94	0.0062		2.3
	hexane	2.20	40	1101	0.012	2500	0.010	1.2	0.0465		1.7	1113	0.018	2500	0.106	1.2	0.0224		1.8
	toluene	2.20	40	1101	0.017	2500	0.015	1.1	0.1093	0.00848	1.9	1113	0.022	2500	0.017	1.0	0.0503	0.00466	2.0
5700	methanol	25.0	40	125	0.012	339	0.016	4.7	0.0064		14	119	0.016	360	0.016	4.5	0.0037		14
	acetone	34.4	40	172	0.019	642	0.019	2.7	0.0335		24	172	0.017	565	0.033	2.5	0.0175		26
	2-propanol	80.2	40	401	0.016	976	0.016	1.1	0.0167		58	401	0.018	984	0.019	1.2	0.0097		56
	hexane	64.7	40	323	0.022	956	0.014	1.4	0.0713		48	323	0.023	909	0.019	1.3	0.371		48
	toluene	64.2	40	321	0.035	920	0.030	1.2	0.1832	-	55	321	0.024	801	0.017	1.2	0.0803		55

[a] Fit in the period of the analyte vapor pulse. [b] Fit over all of the data points in each trace. [c] The optical absorbance averaged across the top of the vapor pulse. [d] Response times, t_r, calculated as $2l^2/D$ using the best fit value of D for each experimental response. [e] $\times 10^8$ cm^2 s^{-1}.

replaced in the upstream analyte flow by either acetone or toluene. If the optical pulse shape in any given experiment either before or after detector resistance versus time data acquisition was not suitably well-defined with an abrupt leading edge, the experimental system was adjusted until the desired pulse shapes were observed and the data were recollected. Fine adjustments in the positioning and alignment of the vapor flow output, the chopper wheel, and the channel housing, all of which were equipped with micropositioners, and slight adjustments of the pumped air flow rate through the inside channel were occasionally required to produce pulses having well-defined abrupt leading edges. A personal computer running applications developed with National Instruments LabVIEW controlled both the flow system and the data acquisition apparatus.

G. Comparison of Calculated and Experimental Resistance versus Time Behavior. All data were processed with programs written in C++. The shape of the pulse profile, which was obtained from the measured analyte optical absorbance versus time of an identical length pulse, was simplified for each experiment to a four point trapezoid shaped curve consisting of a ramp up and a flat period, followed by a ramp down. These values were chosen for each pulse so that the rise and fall slopes would overlay the rise and fall of the optical absorbance signal for each pulse. For the long pulses on the thickest film, where the chopper device was not used and the optical absorbance signal was not recorded, a simple square shaped pulse was used. These pulse profiles essentially provide the boundary condition of eq 3 as a function of time, and the finite difference representations of eq 5,[21,25,26] with $\Delta X = l/40$ and $\Delta T/(\Delta X)^2 = 1$ s cm^{-2}, and eq 11 were then implemented to calculate the time response, S_j, of a detector to a specifically shaped pulse profile:

$$S_j = \frac{R_j - R^i}{R^i} = \frac{1}{\frac{1}{N}\sum_{n=1}^{N}\frac{1}{1 + \Delta R^{eq}/R^i C_{n,j}/C^*}} - 1 \qquad (11)$$

The experimental resistance responses of the detector films were placed on an offset and normalized scale, yielding values for $\Delta R(t)/R^i = (R(t) - R^i)/R^i$. Values of S_j at times that corresponded to the acquisition times of the experimental $R(t)$ data were then extracted from the digital simulation, plotted, and compared to the values of $\Delta R(t)/R^i$ at the times of data acquisition for that specific detector/analyte exposure.

A goodness-of-fit criterion, GOF, comparing each of the M points in the experimental response profile, $\Delta R_m(t)/R^i$ (for $m = 1$ to M), to those in the simulated response profile, S_m, at the same time values was employed to select the best fit value of D, with

$$\mathrm{GOF} = \sqrt{\frac{\sum_{m=1}^{M}\left(\frac{R^i}{\Delta R^{eq}}(S_m - (\Delta R_m(t)/R^i))\right)^2}{(M-1)}} \qquad (12)$$

This process was repeated through several rounds until the goodness-of-fit criterion was no longer significantly minimized. The GOF quantity is displayed in Tables 1 and 2 under the header "full fit", to indicate the relative quality of the fit to the data. The magnitudes of these values for different analyte responses or detectors are comparable because all values were normalized by the value of $\Delta R^{eq}/R^i$ for each exposure. Because these data reflect the totality of each time trace rather than the most meaningful fractions of the pulse, a second value in Tables 1 and 2 under the header "fit" is provided which presents the values of the GOF restricted to the time period of the vapor pulse.

IV. Results

A. Optical Measurement of the Performance of the Vapor Delivery System in the Generation of Short Vapor Pulses. Figure 1 depicts the optical absorbance signals in the vapor path adjacent to a detector film during different length pulses of acetone and toluene vapor. During the shortest-duration pulse, a 17 ms long presentation of acetone vapor, the concentration in the detector chamber reached 90% of its final value within

TABLE 2: Response Times and Effective Film Thickness Calculations for a Minimized Film Thickness PEVA Detector

analyte	P/P_0	pulse length (s)	grid pts, N	fit[a] M	fit[a] GOF	full fit[b] M	full fit[b] GOF	$\Delta R^{eq}/R^i$	A^c	$t_r{}^d$ (s)	$D_{avg}{}^e \times 10^8$ ($cm^2\ s^{-1}$)	$l_{eff}{}^f$ (nm)
methanol	0.10	0.0173	40	867	0.023	2500	0.023	0.0135		0.012	5.9	190
acetone	0.10	0.042	40	1051	0.010	2500	0.016	0.0600	0.0070	0.027	2.2	170
hexane	0.040	0.051	40	1265	0.016	2500	0.020	0.0279		0.041	1.2	150
toluene	0.040	0.088	40	879	0.009	2500	0.016	0.0728	0.0055	0.065	1.0	180

[a] Fit in the period of the analyte vapor pulse. [b] Fit over all of the data points in each trace. [c] The optical absorbance averaged across the top of the vapor pulse. [d] Response times, t_r, were obtained from the best fit curve. [e] Each value of D_{avg} is calculated as the average of the eight D values for the corresponding analyte in Table 1. [f] The effective film thickness l_{eff} is determined for each analyte using D_{avg}.

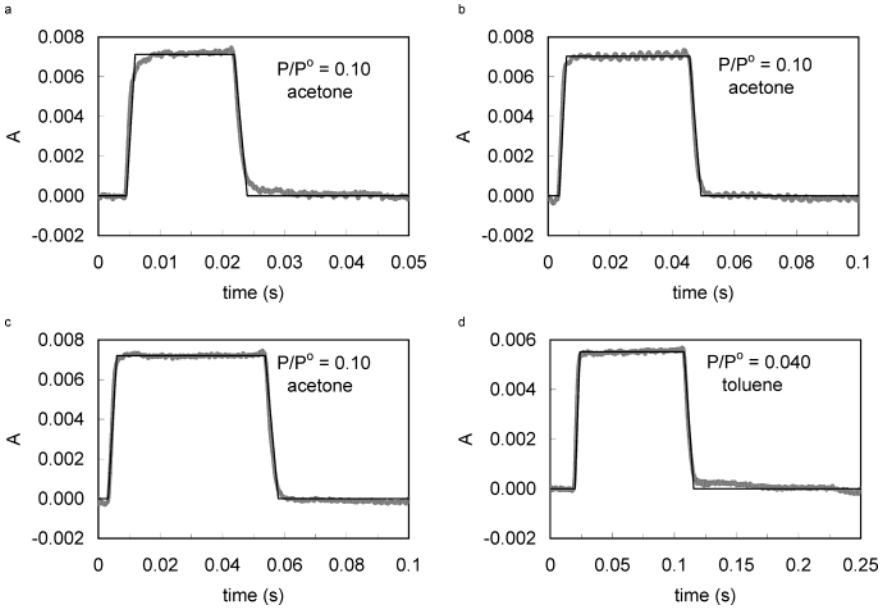

Figure 1. UV optical absorbance of four different length pulses through the channel region adjacent to the detector film: (a) a 17 ms pulse of acetone at $P/P° = 0.10$; (b) a 42 ms pulse of acetone at $P/P° = 0.10$; (c) a 51 ms pulse of acetone at $P/P° = 0.10$; (d) a 88 ms pulse of toluene delivered at $P/P° = 0.040$. The solid line running though the experimental data in each curve is the input parameter used as the surface concentration of analyte to fit the corresponding response curves. All data are the averages of 64 such pulses delivered at a duty cycle of 25%.

<2 ms and reached its maximum value in <5 ms (Figure 1a). Parts b, c, and d of Figure 1 depict the optical responses of slightly longer vapor pulses, having pulse lengths of 42, 51, and 88 ms, respectively. All of the data shown in Figure 1 are the average of 64 nominally identical pulses delivered with a duty cycle of 25%. With the exception of the shortest (17 ms) vapor pulse, the system delivery time for producing a steady-state analyte concentration in the area proximal to the detector was clearly <5% of the pulse width. Detector rise times slower than this value can therefore robustly be ascribed to the detector itself as opposed to the properties of the vapor delivery system, provided that the detectors are measured in response to the shortest pulses possible for that detector to reach steady-state.

B. Time-Dependent Analyte Response Behavior of Carbon−Black Composite Vapor Detectors. Figure 2 displays the relative differential resistance response, $\Delta R(t)/R^i$, for an ultrathin (<200 nm thick by profilometry) PEVA−carbon black composite film exposed to vapor pulses of four different analytes. Each of these analytes was delivered using a pulse of sufficient length such that the detector response displayed a steady-state value by the end of the pulse. The pulses were produced under identical conditions (although not necessarily with the same analyte) to those of the correspondingly lettered pulse of the same length displayed in Figure 1.

Figure 2a displays the $\Delta R(t)/R^i$ response to a 17 ms pulse of methanol at $P/P° = 0.10$, while Figure 2b, c, and d display the detector responses to a 42 ms pulse of acetone at $P/P° = 0.10$, a 51 ms pulse of *n*-hexane at $P/P° = 0.040$, and a 88 ms pulse of toluene at $P/P° = 0.040$, respectively. For acetone and toluene, the optical absorbance data of Figure 1 and resistance response data of Figure 2 were collected simultaneously (i.e. Figure 2b is the detector response vs time to the pulse displayed optically in Figure 1b); however, because methanol and hexane do not exhibit significant absorption in the near-ultraviolet, the forms of these pulses (Figure 1a and c) were recorded separately from the response curves in Figure 2a and c, using acetone and identical flow conditions. The responses of the ultrathin detector were rapid, reaching steady-state in less than 90 ms for these four analytes, and the time required to reach steady-state varied with the identity of the analyte.

C. Comparison between Calculated and Observed Resistance versus Time Profiles. The $\Delta R(t)/R^i$ response was determined for PEVA−carbon black detectors having film thicknesses of 510, 870, 1030, and 5700 nm as measured using profilometry. Each of these four detectors was exposed to pulses of toluene, acetone, methanol, hexane, and 2-propanol at two separate concentrations corresponding to $P/P° = 0.070$ and 0.040, respectively, for a total of 40 separate experiments. The experimental parameters for each of these 40 experiments, including the length of the pulses, are summarized in Table 1. Data for four representative film/analyte combinations, including one sample from each thickness, are displayed in Figures 3−6. Figure 3a displays the response of a 530 nm thick PEVA−carbon black vapor detector to exposure to pulses of two different concentrations of acetone vapor. The optical absor-

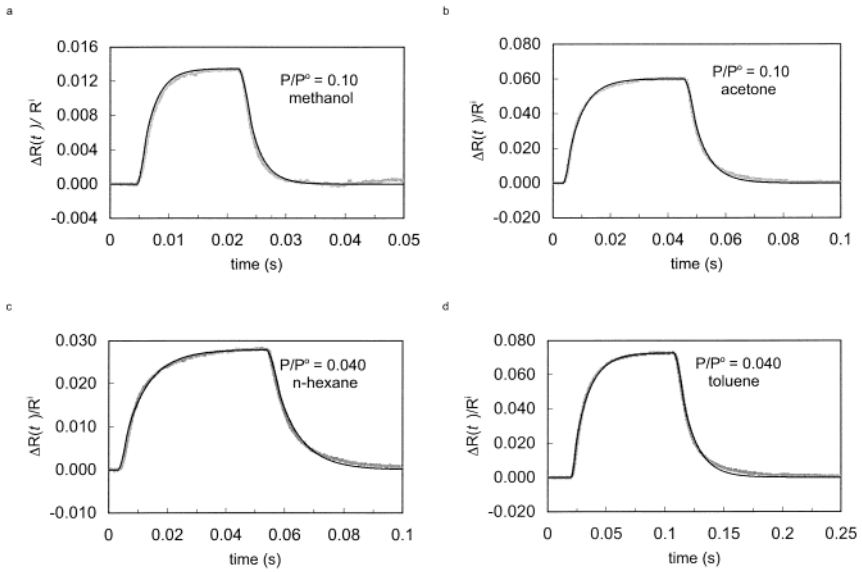

Figure 2. Relative differential resistance responses, $\Delta R(t)/R^i$, (black) of a single ultrathin (<200 nm) PEVA−carbon black composite film exposed to different length pulses of four analyte vapors. The pulses were the same length as those measured optically in Figure 1: (a) a 17 ms pulse of methanol at $P/P^\circ = 0.10$; (b) a 42 ms pulse of acetone at $P/P^\circ = 0.10$; (c) a 51 ms pulse of *n*-hexane at $P/P^\circ = 0.040$; (d) an 88 ms pulse of toluene at $P/P^\circ = 0.040$. All data are the averages of 64 pulses delivered at a duty cycle of 25%. The thick lines running through the experimental data correspond to the best fit calculated response of each curve using the solid lines in Figure 1 to provide the surface concentration.

bances in the air volume adjacent to the detector during these pulses are displayed in Figure 3b. Also shown in Figure 3a are the best fit calculated detector response curves for these $\Delta R(t)/R^i$ values. These fits were calculated using eqs 5 and 11 with the trapezoidally shaped pulse in Figure 3b serving as the film surface boundary condition. As seen in this figure, the data for the sorption and desorption portions of the response were well-fitted using a constant value of *D*, and similar values of *D* were found for the two different analyte concentrations (Table 1).

Figure 4 displays similar data and fits for a 870 nm thick PEVA−carbon black film responding to pulses of methanol vapor. Because methanol does not absorb in the UV, acetone was substituted for the optical measurement of the pulses in Figure 4b, and the optical data were recorded immediately after the methanol detector responses of Figure 4a. Each curve was well-fitted using a single, constant *D* value, and similar *D* values were obtained for the responses produced by exposures to both concentrations of analyte (Table 1). Figure 5 displays similar data and fits for a 1030 nm PEVA−carbon black film to pulses of 2-propanol. Because 2-propanol does not absorb in the UV, toluene was substituted for the optical measurement of the pulses in Figure 5b. Again, each curve was well-fitted to a single constant value of *D*, and similar *D* values were obtained at both concentrations of analyte. Figure 6 displays similar data, but in this case for the response of a 5700 nm thick PEVA−carbon black film to pulses of toluene. The data for the lower-concentration pulse ($P/P^\circ = 0.040$) were well-fitted using a single value of *D*. However, the higher-concentration pulse could not be fitted satisfactorily using this method, and the detector responded more quickly than predicted by the value of *D* used to fit the response to the lower concentration of toluene. This behavior may be indicative of a concentration dependence of *D* for this range of toluene concentration; however, no such effect was observed for the four other film thicknesses of this detector composition.

Table 1 lists the response times for each of the 40 separate analyte/detector combinations investigated. Table 1 also presents the results of fits of all of the data to the digitially simulated

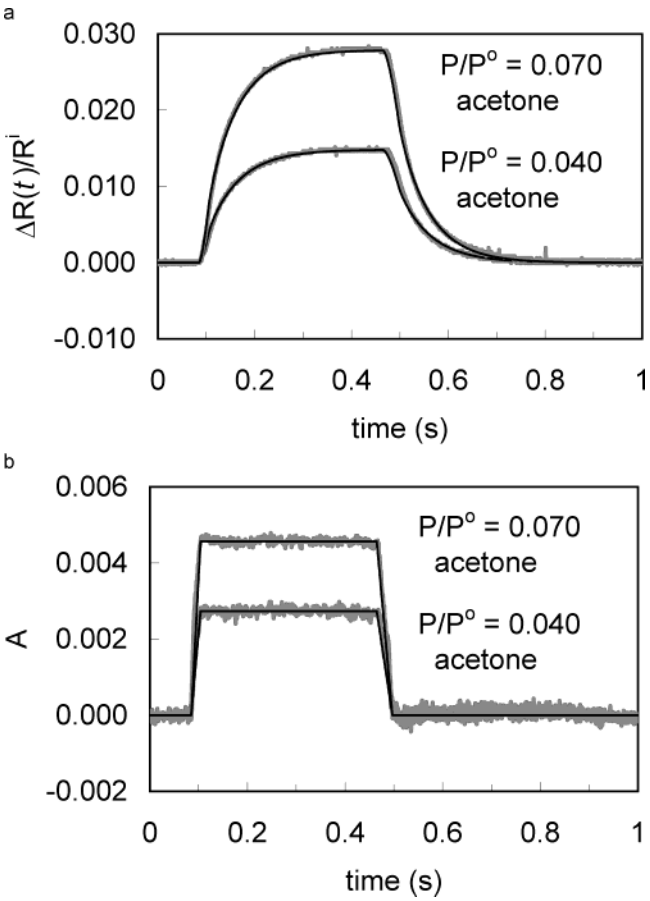

Figure 3. (a) Response of a 510 nm thick PEVA−carbon black detector to the two acetone pulses of part b. The thin solid lines inside the experimental data show the best-fit calculated responses for analyte diffusion into a parallel network of resistors using the thin solid line of part b as the pulse shape. This detector/analyte combination exhibited one of the best overall fits, as indicated by the goodness-of-fit (GOF) parameter. (b) The optical absorbance of the headspace of the chamber directly over the detector film of the two pulses of acetone at $P/P^\circ = 0.040$ and $P/P^\circ = 0.070$, respectively.

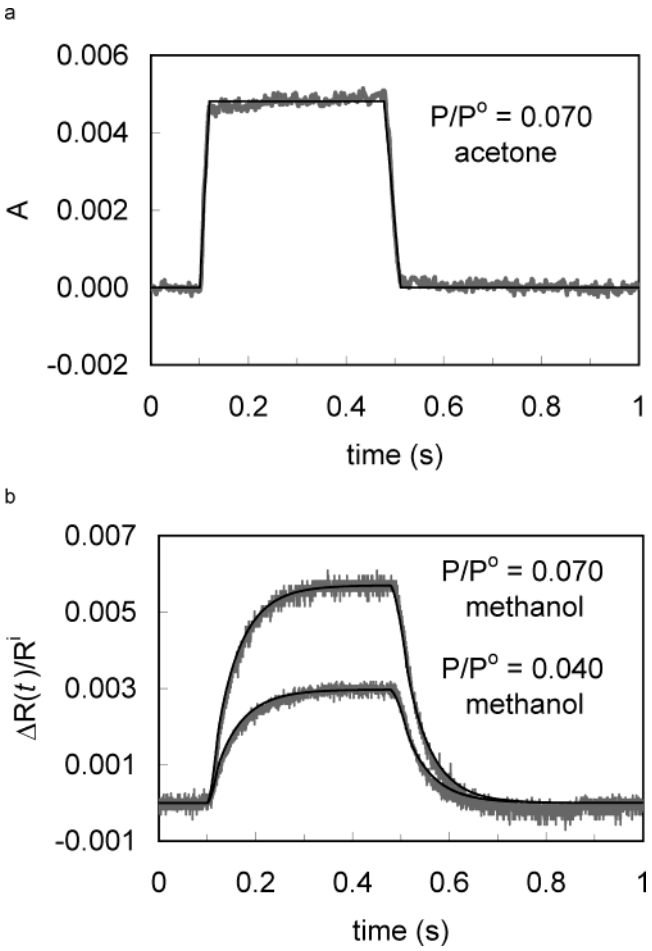

Figure 4. (a) Optical absorbance of the headspace of the chamber directly over the detector film of an acetone pulse delivered at $P/P° = 0.070$. (b) Response of an 870 nm thick PEVA−carbon black detector film to methanol at $P/P° = 0.070$ and $P/P° = 0.040$, respectively. The thin solid lines inside the experimental data of part b show the best fit calculated responses for analyte diffusion into a parallel network of resistors using the thin solid line of part a as the pulse shape. For reference, this detector/analyte combination produced one of the lowest GOF values of all of the data reported in this work.

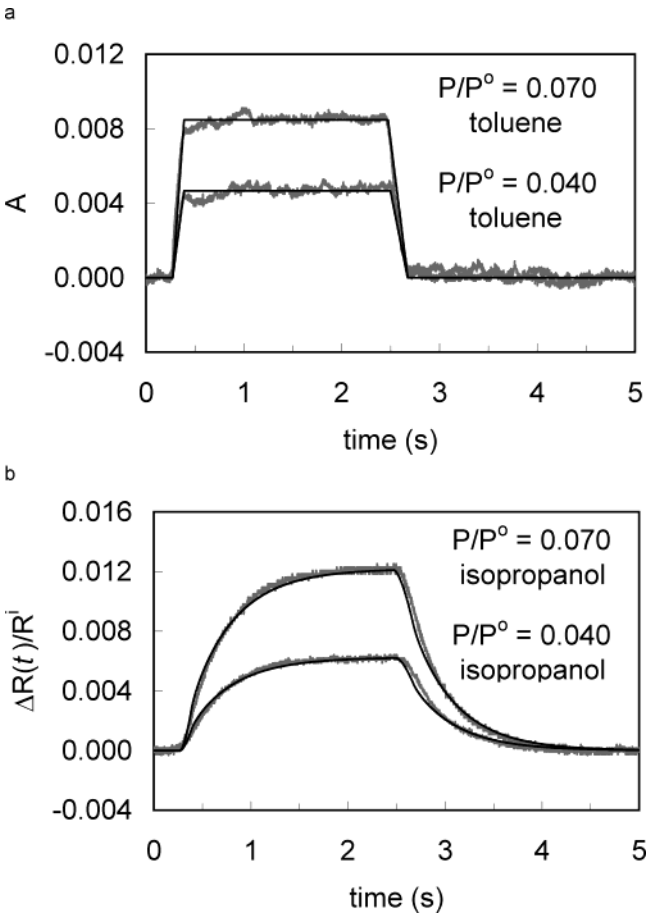

Figure 5. (a) Optical absorbance of the headspace of the chamber directly over the detector film of two pulses of toluene at $P/P° = 0.070$ and $P/P° = 0.040$, respectively. (b) Response of a 1030 nm thick PEVA−carbon black detector to 2-propanol at $P/P° = 0.070$ and $P/P° = 0.040$, respectively. The thin solid lines inside the data show the best-fit calculated responses for analyte diffusion into a parallel network of resistors. This detector/analyte combination exhibited a moderately good overall fit, as indicated by the GOF parameter.

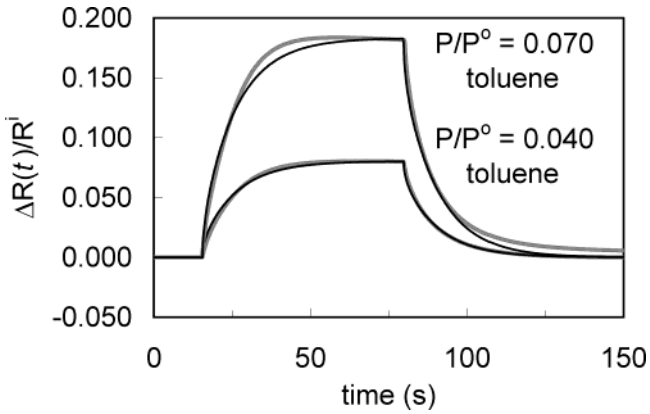

Figure 6. Plot of a 5700 nm thick PEVA−carbon black detector film responding to toluene at $P/P° = 0.070$ and $P/P° = 0.040$, respectively. The thin solid lines inside the experimental data show the best fit calculated responses for analyte diffusion into a parallel network of resistors, assuming a perfect square wave for the pulse shape of analyte vapor striking the detector. The response to toluene at $P/P° = 0.070$ had a poor quality of fit, as reflected by the GOF value, and was visibly the poorest-looking fit of the 44 experiments.

resistance response. The fits were generally good over the entire range of recorded data, and the data recorded at two different analyte concentrations were nearly identically fitted using the same value of D for a given analyte.

D. Response Data and Fits for Ultrathin Detector Films. Figure 2 also shows the best fit calculated responses to experimental data of the ultrathin detector as displayed in that figure. The dark trapezoidal line in the corresponding optical signals of Figure 1 provided the surface boundary condition in each case. However, since the thickness of this film was not clearly defined experimentally, a value of D was not determined from the fitting procedure. Instead, the value of D for each analyte was taken to be the average of eight values of D determined for each analyte/polymer combination from fits of the response data across the four film thickness and two analyte concentrations listed in Table 1. The best fit value of the effective film thickness, l, was then obtained while the value of D was fixed as an input parameter to the model of eq 10. Table 2 displays the results of this effective film thickness calculation, which yielded an average effective film thickness of 180 nm. Table 2 also depicts the goodness of fit criteria and the values of the response times t_r, with t_r defined as the value of $2l^2/D$ (thereby providing a response magnitude within 1% of the equilibrium response) for each of the four analytes of interest. The most rapid t_r value was 12 ms for an ultrathin PEVA−carbon black detector exposed to methanol, while acetone, *n*-hexane, and toluene exhibited response times of 27, 41, and 65 ms, respectively.

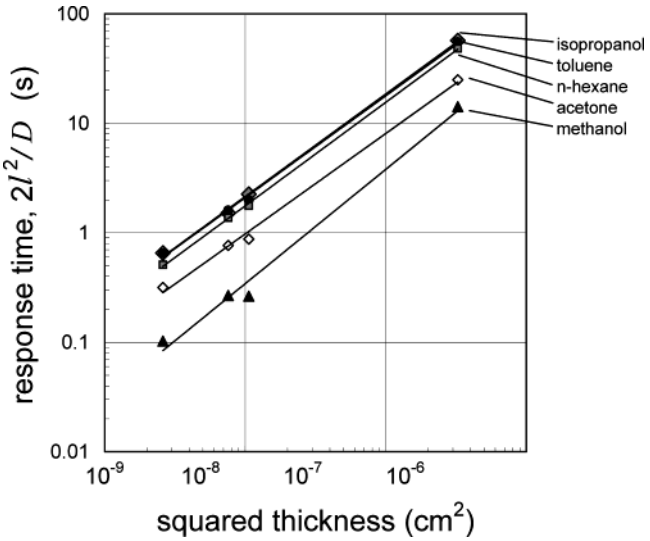

Figure 7. log−log plot of the square of film thickness vs response time (calculated as the value of the film thickness squared × 2 divided by the best fit value of *D*) for the resistance responses of a PEVA−carbon black composite detector film exposed to methanol, acetone, 2-propanol, hexane, and toluene. Each analyte exposure was conducted at two concentrations, and the data for each analyte and film thickness reflect the average of the response times at these two concentrations.

E. Use of Temporal Information To Distinguish between Analytes. Figure 7 displays, on log−log axes, the response times of four PEVA−carbon black composite detectors of different film thicknesses (510, 870, 1030, and 5700 nm) as a function of l^2. Each point is the average of the response times determined for the two concentrations of each analyte at a given film thickness. The linear dependence of response time versus l^2 is in accord with expectations for Fickian analyte diffusion through a finite film thickness and, furthermore, shows that the temporal response can be used to distinguish between analytes on the basis of their different polymer/analyte diffusion coefficients.

V. Discussion

A. Validation of Experimental System Performance. In most studies to date, vapor detectors are held in a chamber under a flow of background gas, and a stream of analyte vapor is introduced into the background flow at a position upstream of the chamber. A significant distance is required to ensure adequate mixing of the two vapor streams before the analyte vapor encounters the detectors. Unfortunately, this requirement, and the volume of the dead space surrounding the detectors, increases the minimum time required to change between the background vapor and the target analyte concentration. In such an experimental configuration, the time response of the vapor delivery system often masks the time response of rapidly responding detectors. For example, in previous work in our laboratory, relatively long exposure times were used to ensure adequate mixing of vapors, to ensure that steady-state concentrations of the vapor in the headspace of the chamber had been achieved prior to measurement of the steady-state $\Delta R^{eq}/R^{i}$ values of the detectors, and to allow the multiplexing ohmmeter to obtain several high precision resistance values on each detector in the array during the period of analyte exposure.[15,16,28]

In this work, we have utilized a vapor delivery system capable of producing multiple pulses of analyte vapor with rapid on/off times, coupled with a system that can independently determine the concentration of analyte in proximity to the vapor sensor. Other olfactometer designs have also incorporated a mechanism for monitoring the shape of the delivered analyte pulse. One such system, developed by Kauer et al.,[19] uses a carrier gas which is doped with CO_2 when the analyte is present. Although this design has the advantage of doping any analyte vapor with the CO_2 marker, it has the disadvantage of providing only indirect information on the magnitude of the analyte concentration of interest. Similar to the design described herein, the Kauer olfactometer also uses a design principle based on quickly switching between multiple vapor streams; however, the solenoid valve and limited flow volumes employed in that design would prohibit switching the analyte concentrations over large area (≈0.1 cm^2) sensor films at the fastest off/on times (<5 ms) required for experiments on the most rapidly responding vapor detectors investigated herein.

As exhibited by the absorbance data of Figure 1, the chopper-coupled chamber was able to effect a rapid switch between the background air and analyte vapor streams. As the chopper wheel sweeps at a given rotational velocity across the opening to the detector housing channel, the maximum rise/fall time of the pulse is limited by the dimensional component of the channel tangential to the arc of the wheel. This value corresponds to the 0.2 cm height of the channel opening divided by the approximately 6.8 cm arc length of the opening in the chopper wheel. For the current design, this geometric factor produces a minimum analyte rise time of about 3% of the pulse length and a minimum analyte fall time of the same fraction. Most analyte pulses used in our experiments reached maximum concentration values in 4−5% of the pulse length, as shown by the data of Figure 1b−d and Figures 3a, 4a, 5a, and 6a. At the end of the pulse, the analyte concentration fell to zero almost as quickly, but a slight trail off of the last ∼5% of the amplitude was evident in several of the experiments. Larger chopper wheels or smaller channel openings may permit the realization of yet more rapid on/off times.

For very fast pulses, the minimum achievable rise time of our experimental setup was limited by a separate phenomenon. Both the active region of the detector films and the optical path through the chamber have dimensional components along the primary direction of the air flow. This dimension of ≈1.0 cm was, in general, negligible with respect to the speed that the pulse edge moved along the channel. For example, at a volumetric flow of 5.9 L min^{-1}, the pulse edge moved through the 0.06 cm^2 cross section of the channel at a linear flow rate of 1.65×10^3 cm s^{-1}. Assuming that the pulse front does not broaden significantly, a 1 cm long detector would experience an integration of the edge of a 10 ms vapor pulse that would limit the effective pulse rise time to about 6% of the pulse width. This broadening effect only influences the shortest of pulses and may be partially visible in the 17 ms pulse in Figure 1a, which was the shortest pulse width used in our experiments. However, most of the pulses used in this study were much longer in duration, and such pulses were limited only by the fractional rise/fall times described above. This chopper system would also be useful for evaluating the response times of some other detector methodologies such as tin oxide, metal-oxide-semiconductor field-effect transistor (MOSFET), surface acoustic wave, quartz crystal microbalance, and conducting polymer sensor modalities.

B. Performance of an Ultrathin PEVA−Carbon Black Detector. Figure 2 displays the $\Delta R(t)/R^{i}$ response of an ultrathin polymer composite detector film upon exposure to organic vapors. The PEVA−carbon black detector of Figure 2 reached steady-state (i.e. the region where each curve levels off at its equilibrium value of $\Delta R^{eq}/R^{i}$) extremely rapidly. This detector attained a steady-state response in less than 85 ms for exposures

to methanol, acetone, *n*-hexane, and toluene. This ultrathin film was spray cast onto the substrate with just enough passes (typically 5) of an airbrush to produce a measured resistance value of <1 MΩ. This resistance value was desired to ensure less than a 1:100 input impedance ratio relative to the 100 MΩ input impedance of the preamplifier used in these experiments. A different electrode geometry with more closely spaced electrodes may permit the use of still thinner films producing still more rapid response times if so desired.

At the quoted response times in Table 1, the response magnitudes are within 1% of the true equilibrium values. The degree to which a detector must approach its equilibrium value for a given application depends on the level of acceptable error in the signal amplitude. If a 10% underestimation of the response is acceptable, as may be the case in tasks such as in discrimination between structurally very different analytes, then significantly less time is required to reach an acceptable degree of certainty in the signal amplitude than the response times listed in Tables 1 and 2. For example, the detector of Figure 2 produced a response to 90% of its steady-state value within only 7 ms for the fastest-responding analyte, methanol, and within 30 ms for the slowest-responding analyte, toluene. An array of similarly rapidly responding detectors composed of different polymers would permit classification or discrimination tasks for analytes with similar values of D in less than 30 ms, which would be more than rapid enough for real time analysis of vapor levels with a portable or wand-type device.

C. Comparison of Calculated and Experimental Response versus Time Curves. The behavior of the $\Delta R(t)/R^i$ data recorded in this work was remarkably well-fitted through use of a simple Fickian diffusion model with a constant diffusion coefficient for the analyte as a function of both time and analyte concentration in the PEVA−carbon black composite films. Comparisons of the predicted response profile to the experimental data were made by comparing simulated curves calculated with a range of D values to the experimental data and then repeating the process through several successive rounds. In general, as summarized in Tables 1 and 2, the fits obtained using the model of eqs 3−10 were extremely satisfactory. However, a more complicated treatment will likely be required for some other types of polymer−carbon black composites, which sometimes exhibit drift and more complex response curves in a reflection of non-Fickian behavior under at least some analyte concentration conditions. For ultrathin carbon black−polymer composites, the size of the carbon black particles may become important and could produce a complex resistance response, possibly even behaving as a 2-dimensional network model instead of a 3-dimensional network model, even for systems such as those studied herein which exhibit Fickian diffusivity through a 3-dimensional network model on larger thickness and time scales.

Diffusion coefficients for the polymer, analyte, and temperature conditions used in these experiments are not apparently available in the literature, but the values extracted from the modeling appear reasonable when compared to those of similar analytes diffusing into somewhat similar polymers. For sorption of methanol into PEVA−carbon black composite detectors, the average diffusion coefficient measured for two analyte concentrations of $P/P^\circ = 0.070$ and $P/P^\circ = 0.040$ into each of the four film thickness (510, 870, 1025, and 5700 nm) was $(5.8 \pm 1.4) \times 10^{-8}$ cm^2 s^{-1}. This value is reasonably similar to the reported value of 1.5×10^{-9} cm^2 s^{-1} for diffusion of methanol into poly(vinyl acetate) at 298 K.[22] The values of diffusion coefficients of a given molecule can vary significantly from polymer to polymer, and the value for methanol diffusion into a more chemically dissimilar polymer, poly(methyl acrylate), at 303 K has been reported to be 1.0×10^{-7} cm^2 s^{-1}.[22]

D. Implications for Vapor Sampler Design. The chopper-coupled detector setup allows frequent referencing of the detector from a vapor response to its baseline response magnitude in zero or background gas by switching between two air streams where only one of those streams comes from the source of sampled analyte vapor. This approach would be useful for any type of vapor detector exhibiting large amounts of baseline drift because it permits ready separation of the signal into its analyte-induced component and its baseline component. The noise error of a given measurement average decreases with the square root of the number of repetitions, provided that the source of the noise is asynchronous to the period of measurement. Because the chopper device permits averaging of a large number of pulses, the noise error during a given measurement time can therefore be reduced. The traces exhibited in Figure 2 show little noise even though they were measured on a very small volume film, which reflects in part the fact that they were averaged over 64 measurements during the observation time. All parts of the device which are displayed in Scheme 1 could be easily made portable and lend themselves readily to miniaturization and incorporation into a sampling device. Of course, this approach is only beneficial when the detectors respond sufficiently rapidly so as to follow the oscillations in analyte concentration effected by the sampling wheel, as is clearly the case for the detector/analyte combinations investigated in this study.

VI. Conclusions

The resistance response versus time profiles of PEVA−carbon black composite vapor detectors were well-fitted to a model that employed a one-dimensional, constant, diffusion coefficient of analyte into a network of parallel layers wherein the resistance of each layer is proportional to the local concentration of analyte. The resistance response times of a given polymer/analyte combination were shown to be proportional to the square of the film thickness for detectors having five different film thicknesses. An ultrathin PEVA−carbon black detector, having an effective thickness of 180 nm, produced response times of 12 ms in response to methanol and responded within 65 ms to all four of the organic vapors tested in this work. Temporal modulation of the analyte concentration permits ready separation of the signal into its analyte-induced component and its baseline component, leading to a reduction in the noise error of a given average analyte response measurement during a fixed measurement time. Such carbon black−polymer composite vapor detectors can thus exhibit sufficiently rapid response times to detect and classify organic vapors in real time under ambient temperature and pressure conditions.

Acknowledgment. We acknowledge the NIH and an Army MURI for support of this work.

Supporting Information Available: Dimensioned drawings of the aluminum housing, the aluminum chopper wheels, and the glass substrates. This material is available free of charge via the Internet at http://pubs.acs.org.

References and Notes

(1) Lonergan, M. C.; Severin, E. J.; Doleman, B. J.; Beaber, S. A.; Grubbs, R. H.; Lewis, N. S. *Chem. Mater.* **1996**, *8*, 2298−2312.

(2) Shurmer, H. V.; Corcoran, P.; Gardner, J. W. *Sens. Actuator, B: Chem.* **1991**, *4*, 29−33.

(3) Pearce, T. C.; Gardner, J. W.; Friel, S.; Bartlett, P. N.; Blair, N. *Analyst* **1993**, *118*, 371−377.
(4) Freund, M. S.; Lewis, N. S. *Proc. Natl. Acad. Sci. U.S.A.* **1995**, *92*, 2652−2656.
(5) Slater, J. M.; Watt, E. J. *Analyst* **1991**, *116*, 1125−1130.
(6) Grate, J. W.; Martin, S. J.; White, R. M. *Anal. Chem.* **1993**, *65*, A987−A996.
(7) Grate, J. W.; Martin, S. J.; White, R. M. *Anal. Chem.* **1993**, *65*, A940−A948.
(8) Cornila, C.; Hierlemann, A.; Lenggenhager, R.; Malcovati, P.; Baltes, H.; Noetzel, G.; Weimar, U.; Gopel, W. *Sens. Actuator, B: Chem.* **1995**, *25*, 357−361.
(9) Johnson, S. R.; Sutter, J. M.; Engelhardt, H. L.; Jurs, P. C.; White, J.; Kauer, J. S.; Dickinson, T. A.; Walt, D. R. *Anal. Chem.* **1997**, *69*, 4641−4648.
(10) Dickinson, T. A.; White, J.; Kauer, J. S.; Walt, D. R. *Nature* **1996**, *382*, 697−700.
(11) White, J.; Kauer, J. S.; Dickinson, T. A.; Walt, D. R. *Anal. Chem.* **1996**, *68*, 2191−2202.
(12) Severin, E. J.; Lewis, N. S. *Anal. Chem.* **2000**, *72*, 2008−2015.
(13) Lu, C. *Applications of Piezoelectric Quartz Crystal Microbalances*; Elsevier: New York, 1984.
(14) Albert, K. J.; Lewis, N. S.; Schauer, C. L.; Sotzing, G. A.; Stitzel, S. E.; Vaid, T. P.; Walt, D. R. *Chem. Rev.* **2000**, *100*, 2595−2626.
(15) Severin, E. J.; Doleman, B. J.; Lewis, N. S. *Anal. Chem.* **2000**, *72*, 658−668.
(16) Doleman, B. J.; Lonergan, M. C.; Severin, E. J.; Vaid, T. P.; Lewis, N. S. *Anal. Chem.* **1998**, *70*, 4177−4190.
(17) Briglin, S. M.; Freund, M. S.; Tokumaru, P.; Lewis, N. S. *Sens. Actuator, B: Chem.* **2002**, *82*, 54−74.
(18) Tobias, P.; Baranzahi, A.; Spetz, A. L.; Kordina, O.; Janzen, E.; Lundstrom, I. *IEEE Electron Device Lett.* **1997**, *18*, 287−289.
(19) Kauer, J. S.; Shepherd, G. M. *Brain Res.* **1975**, *85*, 108−113.
(20) Briglin, S. M.; Burl, C. M.; Freund, M. S.; Lewis, N. S.; Matzger, A.; Ortiz, D. N.; Tokumaru, P. *Proc. SPIE—Int. Soc. Opt. Eng.* **2000**, *4038*.
(21) Crank, J. *The Mathematics of Diffusion*; Clarendon Press: Oxford, 1975.
(22) Fujita, H. *Diffusion in Polymers*; Academic Press: New York, 1968.
(23) Vrentas, J. S.; Vrentas, C. M. *Chem. Eng. Sci.* **1998**, *53*, 629−638.
(24) Vrentas, J. S.; Vrentas, C. M. *J. Polym. Sci., Part B: Polym. Phys.* **2001**, *39*, 1529−1547.
(25) Press, W. H.; Teukolsky, S. A.; Vetterling, W. T.; Flannery, B. P. *Numerical Recipes in C*, 2nd ed.; Cambridge University Press: New York, 1997.
(26) Smith, G. D. *Numerical Solution of Partial Differential Equations: Finite Difference Methods*, 3rd ed.; Cambridge University Press: New York, 1985.
(27) Doleman, B. J.; Severin, E. J.; Lewis, N. S. *Proc. Natl. Acad. Sci. U.S.A.* **1998**, *95*, 5442−5447.
(28) Doleman, B. J.; Sanner, R. D.; Severin, E. J.; Grubbs, R. H.; Lewis, N. S. *Anal. Chem.* **1998**, *70*, 2560−2564.